Testing unification and dark matter with gravitational waves

Bartosz Fornal, Kassandra Garcia, and Erika Pierre
Department of Chemistry and Physics, Barry University, Miami Shores, Florida 33161, USA

(Received 25 May 2023; accepted 25 August 2023; published 20 September 2023)

We propose to search for a new type of gravitational wave signature relevant for particle physics models with symmetries broken at vastly different energy scales. The spectrum contains a characteristic double-peak structure consisting of a sharp peak from domain walls and a smooth bump from a first order phase transition in the early universe. We demonstrate how such a gravitational wave signal arises in a new theory unifying baryon number and color into an SU(4) gauge group broken at the multi-TeV scale, and with the lepton number promoted to an SU(2) gauge symmetry broken at the multi-EeV scale. The model contains two types of dark matter particles, explains the observed domination of matter over antimatter in the Universe, and accommodates nonzero neutrino masses. We discuss how future gravitational wave experiments, such as LISA, Big Bang Observer, DECIGO, Einstein Telescope, and Cosmic Explorer, can be utilized to look for this novel signature.

DOI: 10.1103/PhysRevD.108.055022

I. INTRODUCTION

The Standard Model of elementary particle physics is a gauge theory based on the symmetry group

$$\mathrm{SU}(3)_c \times \mathrm{SU}(2)_L \times \mathrm{U}(1)_Y. \tag{1}$$

The electroweak sector of the theory was formulated in the 1960s [1–5], whereas the quantum chromodynamics part was constructed in the 1970s [6–8]. Since then, the model has withstood all experimental tests, culminating in the discovery of the Higgs particle at the Large Hadron Collider in 2012 [9,10]. Despite this huge success, the Standard Model on its own is not complete, since it does not accommodate the following: (a) dark matter, (b) matter-antimatter asymmetry of the Universe, and (c) nonzero neutrino masses.

The symmetry structure in Eq. (1) is rather complex and its origins are not understood. There is no theoretical reason to expect that this exact gauge symmetry persists all the way up to the Planck scale. Indeed, the Standard Model symmetry might be just a low-energy manifestation of a larger gauge group existing at higher energy scales, just as $\mathrm{U}(1)_{\mathrm{EM}}$ is a leftover symmetry from the breaking of $\mathrm{SU}(2)_L \times \mathrm{U}(1)_Y$ at the electroweak scale. Additionally, the outstanding open questions require new fields to be introduced into the theory—such new fields would most naturally be part of a gauge structure beyond that of the Standard Model.

Specifically, the evidence for the existence of dark matter has piled up over the past decades [11–13], but the strength of its interactions with the Standard Model remains unknown, with only upper limits set by various experiments (for a review, see [14]). Although the pessimistic scenario, in which the dark matter particle is completely decoupled from the Standard Model, is a viable possibility, the hope is that the dark matter actually constitutes an integral part of a larger particle physics structure involving nonzero interactions with the known particles. In such a case, there must exist a gauge symmetry describing how the dark matter fits into the entire particle physics picture. This framework could also offer explanations for other pressing problems, such as the origin of the matter-antimatter asymmetry of the Universe or the mechanism behind neutrino masses.

In this work, we propose a new gauge extension of the Standard Model which accomplishes the above-mentioned goals, adopting elements of the models constructed in [15,16]. This theory contains two possible GeV-scale candidates for the dark matter particle, while the observed excess of matter over antimatter is explained in an asymmetric dark matter setting; i.e., the dark matter and ordinary matter asymmetries share a common origin [17–22]. The out-of-equilibrium dynamics needed for a successful baryogenesis/leptogenesis is provided by two first order phase transitions in the early universe. The energy scales for those phenomena are free parameters, and we consider the scenario in which both of them are high, inaccessible at the Large Hadron Collider. However, such high symmetry breaking scales make the model ideal for being probed in gravitational wave experiments.

Indeed, the much needed breakthrough in particle physics might come from the detection of primordial gravitational waves. Thus far, the Laser Interferometer Gravitational Wave Observatory (LIGO) within the LIGO/Virgo Collaboration has discovered signals coming from black hole/neutron star mergers [23]; however, a stochastic gravitational wave background from the early universe is predicted by many models of physics beyond the Standard Model. Although LIGO is currently sensitive to a relatively small parameter space of such models, the reach will be considerably improved with future upgrades, as well as other planned gravitational wave experiments, such as the Laser Interferometer Space Antenna (LISA) [24], Big Bang Observer (BBO) [25], DECIGO [26], Einstein Telescope (ET) [27], and Cosmic Explorer (CE) [28]. The possible sources for this stochastic gravitational wave signal are the following: first order phase transitions in the early universe after inflation [29], inflation itself [30], and topological defects (domain walls [31] and cosmic strings [32,33]). In the model we propose, gravitational waves originate from annihilating domain walls and a first order phase transition.

Domain walls are topological defects which are created when a discrete symmetry is spontaneously broken [34]. They exist around boundaries of regions corresponding to different vacua. Stable domain wall configurations would lead to cosmological problems, since they would overclose the Universe. However, if the two vacua have different energy densities (this difference is called the potential bias), then domain walls become unstable and annihilate, leading to a stochastic gravitational wave background, *a priori* measurable today. This can be realized in many particle physics scenarios, e.g., electroweak-scale new physics [35–38], supersymmetry [39], Peccei-Quinn symmetry [40–44], high-scale leptogenesis [45], left-right symmetry [46,47], flavor symmetries [48], grand unification [49], or thermal inflation [50]. A review of domain walls and the resulting gravitational wave signatures are discussed in [51].

The other sources of a stochastic gravitational wave background are cosmological first order phase transitions, which occur when the effective potential of the theory develops a minimum at a nonzero field vacuum expectation value separated by a potential barrier from the high temperature minimum at zero field value. The transition process from the high temperature false vacuum to the newly formed true vacuum corresponds to bubbles being nucleated in various points in space, which then expand and fill up the entire Universe. The violent expansion of the bubbles results in sound shock waves in the primordial plasma. This, accompanied by bubble collisions and turbulence, leads to the emission of gravitational radiation. The literature on the subject is extensive and involves various particle physics theories, e.g., electroweak-scale extensions of the Standard Model [52–60], dark gauge groups [61–64], dark matter [65–71], axions [72–74], grand unification [75–77], conformal invariance [78,79], supersymmetry [80,81], left-right symmetry [47,82,83], seesaw mechanism [84–87], baryon/lepton number violation [88,89]), new flavor physics [90,91], and leptogenesis [92,93]. If a transition is strongly supercooled [94–96], the signal can be searched for in LIGO/Virgo/KAGRA datasets [97]. For a review of gravitational waves from first order phase transitions see [98,99].

In the model we construct, there are two gauge symmetries that are broken at vastly different energy scales. Due to the shape of the effective potential, the first order phase transition happening at a high energy scale ($\sim$100 EeV) leads to the creation of domain walls, whose subsequent annihilation produces a stochastic gravitational wave background peaked in the frequency range relevant for the Einstein Telescope and Cosmic Explorer. The phase transition happening at a lower energy scale ($\sim$100 TeV) is also first order and results in a gravitational wave signal within the sensitivity range of LISA, Big Bang Observer, and DECIGO. The theory is unique since there are two dark matter candidates and the matter-antimatter asymmetry can be produced in an asymmetric dark matter framework both at the high and low symmetry breaking scales. Because of this, the dark matter mass does not have to be $\sim$1.75 GeV (as in [15]) or $\sim$5 GeV (as in [16]), but it can well be $\lesssim$1 GeV, possibly leading to intriguing connections to nuclear physics through the appearance of a neutron dark decay channel.

We begin by formulating the model in Sec. II, including the symmetry breaking pattern, particle content, masses, and couplings. Then, in Secs. III and IV we discuss the dark matter candidates, as well as the mechanism for leptogenesis at the high scale and baryogenesis at a lower scale. This is followed by a derivation of the expected stochastic gravitational wave signal from domain walls (Sec. V) and the first order phase transition (Sec. VI). The novel signature involving a combination of the two signals is discussed in Sec. VII and followed by conclusions in Sec. VIII.

II. MODEL

To illustrate the novel gravitational wave signature, we consider a new model combining the features of theories proposed in [15,16]. The model is based on the gauge symmetry

$$\mathrm{SU}(4) \times \mathrm{SU}(2)_L \times \mathrm{U}(1)_X \times \mathrm{SU}(2)_\ell, \tag{2}$$

where the SU(4) group unifies color with baryon number, $\mathrm{SU}(2)_\ell$ corresponds to a generalized lepton number, and X is a linear combination of the diagonal generator of SU(4) and the hypercharge. Below we discuss the symmetry breaking pattern and the particle content of the model, along with the particle masses and couplings relevant for the subsequent analysis of the gravitational wave signal.

A. Symmetry breaking

The model exhibits a two-step symmetry breaking pattern. We assume that the $SU(2)_\ell$ group is broken first at a very high scale $\sim 10^8$ TeV, with a subsequent breaking of SU(4) at a lower scale ~100 TeV down to the Standard Model:

$$\begin{gathered}\mathrm{SU}(4)\times\mathrm{SU}(2)_L\times\mathrm{U}(1)_X\times\mathrm{SU}(2)_\ell\\ \downarrow\sim 100\ \mathrm{EeV}\\ \mathrm{SU}(4)\times\mathrm{SU}(2)_L\times\mathrm{U}(1)_X\\ \downarrow\sim 100\ \mathrm{TeV}\\ \mathrm{SU}(3)_c\times\mathrm{SU}(2)_L\times\mathrm{U}(1)_Y.\end{gathered}$$

This choice for the symmetry breaking scales is very different than previously considered in the literature, where they were chosen to be ~TeV for SU(4) breaking in [15] and $SU(2)_\ell$ breaking in [16], and ~10 PeV for $SU(2)_\ell$ breaking in [69].

To implement the above symmetry breaking pattern, as in [16] we introduce two $SU(2)_\ell$ doublet scalars, denoted here by $\hat{\Psi}_1$ and $\hat{\Psi}_2$, governed by the tree-level potential

$$\begin{aligned}V_\Psi(\hat{\Psi}_1,\hat{\Psi}_2) = &-m_1^2|\hat{\Psi}_1|^2 - m_2^2|\hat{\Psi}_2|^2 - (m_{12}^2\hat{\Psi}_1^\dagger\hat{\Psi}_2 + \mathrm{H.c.})\\ &+\lambda_1|\hat{\Psi}_1|^4+\lambda_2|\hat{\Psi}_2|^4+\lambda_3|\hat{\Psi}_1|^2|\hat{\Psi}_2|^2\\ &+\lambda_4|\hat{\Psi}_1^\dagger\hat{\Psi}_2|^2+[(\tilde{\lambda}_5|\hat{\Psi}_1|^2+\tilde{\lambda}_6|\hat{\Psi}_2|^2\\ &+\tilde{\lambda}_7\hat{\Psi}_1^\dagger\hat{\Psi}_2)\hat{\Psi}_1^\dagger\hat{\Psi}_2+\mathrm{H.c.}].\end{aligned}\tag{3}$$

Those scalars develop vacuum expectation values

$$\langle\hat{\Psi}_i\rangle = \frac{1}{\sqrt{2}}\begin{pmatrix}0\\ v_i\end{pmatrix}\tag{4}$$

breaking the $SU(2)_\ell$ group and reducing the symmetry to $\mathrm{SU}(4)\times\mathrm{SU}(2)_L\times\mathrm{U}(1)_X$. It is convenient to define

$$v_\Psi \equiv \sqrt{v_1^2+v_2^2}.\tag{5}$$

There are five physical scalar components of $\hat{\Psi}_1$ and $\hat{\Psi}_2$, and three gauge bosons from $SU(2)_\ell$ breaking.

The second stage of symmetry breaking occurs when the SU(4) quadruplet scalar $\hat{\Phi} = (4,1,\frac{1}{2},1)$, subject to the tree-level potential

$$V_\Phi(\hat{\Phi}) = -m_\Phi^2|\hat{\Phi}|^2+\lambda_\Phi|\hat{\Phi}|^4,\tag{6}$$

develops the vacuum expectation value [15]

$$\langle\hat{\Phi}\rangle = \frac{1}{\sqrt{2}}(\,0\quad 0\quad 0\quad v_\Phi\,)^T.\tag{7}$$

This breaks the symmetry down to the Standard Model gauge group, with the hypercharge emerging as a combination of X and the diagonal SU(4) generator T^{15},

$$Y = X+\frac{1}{6}\mathrm{diag}(1,1,1,-3).\tag{8}$$

The SU(4) breaking leads to seven massive gauge bosons—six of them form three complex vector fields G' transforming as color triplets, and one is the neutral gauge boson Z'.

Along with the condition $v_\Psi \gg v_\Phi$, we assume that the coefficients of the cross terms between the $\hat{\Psi}_i$ and $\hat{\Phi}$ fields in the scalar potential are small, and thus the two symmetry breaking phenomena can be considered independently of each other.

B. Fermionic particle content

Given the structure of the theory, the Standard Model quarks Q_L, u_R, and d_R are singlets under $SU(2)_\ell$, but they constitute part of SU(4) quadruplets,

$$\begin{aligned}\hat{Q}_L &\equiv (\,Q_L^r\quad Q_L^b\quad Q_L^g\quad \tilde{Q}_L\,)^T = (4,2,0,1),\\ \hat{u}_R &\equiv (\,u_R^r\quad u_R^b\quad u_R^g\quad \tilde{u}_R\,)^T = \left(4,1,\frac{1}{2},1\right),\\ \hat{d}_R &\equiv (\,d_R^r\quad d_R^b\quad d_R^g\quad \tilde{d}_R\,)^T = \left(4,1,-\frac{1}{2},1\right).\end{aligned}\tag{9}$$

The Standard Model leptons l_L and e_R, and the right-handed neutrino ν_R (leading to Dirac masses for the neutrinos), on the other hand, are singlets under SU(4), but they are part of $SU(2)_\ell$ doublets,

$$\begin{aligned}\hat{l}_L &\equiv (\,l_L\quad \tilde{l}_L\,)^T = \left(1,2,-\frac{1}{2},2\right),\\ \hat{e}_R &\equiv (\,e_R\quad \tilde{e}_R\,)^T = (1,1,-1,2),\\ \hat{\nu}_R &\equiv (\,\nu_R\quad \tilde{\nu}_R\,)^T = (1,1,0,2).\end{aligned}\tag{10}$$

To cancel the resulting gauge anomalies, we introduce the same $SU(2)_\ell$ and SU(4) singlet fields as in [15,16], i.e., $Q'_R = (1,2,-\frac{1}{2},1)$, $u'_L = (1,1,0,1)$, $d'_L = (1,1,-1,1)$, $l'_R = (1,2,-\frac{1}{2},1)$, $e'_L = (1,1,-1,1)$, $\nu'_L = (1,1,0,1)$, for each generation separately.

C. Particle masses and couplings

These $SU(2)_\ell$ and SU(4) singlet fields allow all beyond–Standard Model fermions to have vectorlike masses,

$$\begin{aligned}\mathcal{L}_Y = \sum_i (&Y_l^{ab}\bar{\tilde{l}}_L^a \hat{\Psi}_i l'^b_R + Y_e^{ab}\bar{\tilde{e}}_R^a \hat{\Psi}_i e'^b_L + Y_\nu^{ab}\bar{\tilde{\nu}}_R^a \hat{\Psi}_i \nu'^b_L) \\ &+ Y_Q^{ab}\bar{\hat{Q}}_L^a \hat{\Phi} Q'^b_R + Y_u^{ab}\bar{\hat{u}}_R^a \hat{\Phi} u'^b_L + Y_d^{ab}\bar{\hat{d}}_R^a \hat{\Phi} d'^b_L \\ &+ y_e^{ab}\bar{\tilde{l}}_L^a H \hat{e}_R^b + y_\nu^{ab}\bar{\tilde{l}}_L^a \tilde{H} \hat{\nu}_R^b + y'^{ab}_e \bar{l}'^a_R H e'^b_L \\ &+ y'^{ab}_\nu \bar{l}'^a_R \tilde{H} \nu'^b_L + y_u^{ab}\bar{\hat{Q}}_L^a \tilde{H} \hat{u}_R^b + y_d^{ab}\bar{\hat{Q}}_L^a H \hat{d}_R^b \\ &+ y'^{ab}_u \bar{Q}'^a_R \tilde{H} u'^b_L + y'^{ab}_d \bar{Q}'^a_R H d'^b_L + \text{H.c.}\end{aligned} \tag{11}$$

For order one Yukawas, this results in ∼100 EeV masses for fermions coupling to $\hat{\Psi}_i$ and ∼100 TeV for those interacting with $\hat{\Phi}$. In order to have viable asymmetric dark matter candidates, as will be discussed in Sec. IV, some of the Yukawas need to be small, leading to ∼GeV dark matter masses.

The Standard Model masses for quarks and leptons are generated by the Yukawa matrices y_d, y_u, and y_e, whereas the neutrinos get their masses from y_ν. The terms involving the Higgs also lead to additional contributions to the new fermion masses, so, in general, one would need to worry about constraints from electroweak precision data. However, due to the high scales of $\mathrm{SU}(2)_\ell$ and SU(4) symmetry breaking, it is phenomenologically natural to assume

$$\begin{aligned} Y_{l,e,\nu} v_\Psi &\gg y_{e,\nu} v_H, \qquad & Y_{l,e,\nu} v_\Psi &\gg y'_{e,\nu} v_H, \\ Y_{Q,u,d} v_\Phi &\gg y_{u,d} v_H, \qquad & Y_{Q,u,d} v_\Phi &\gg y'_{u,d} v_H, \end{aligned} \tag{12}$$

where $v_H = 246$ GeV, which implies that the values of the precision electroweak observables are consistent with their Standard Model predictions.

The mass matrices for the components of $\hat{\Psi}_1$ and $\hat{\Psi}_2$ (i.e., P_1, P_2, A, C_1, C_2) were derived in [69], and result in large masses for all the scalars except for A, whose mass is fine-tuned to be small, ∼GeV, achieved when the parameters of the model satisfy $\mathrm{Re}(m_{12}^2) \simeq 2|\tilde{\lambda}_7| v_1 v_2$. In addition, bounds on Higgs decays from the Large Hadron Collider require the appropriate tree-level Lagrangian terms describing the interactions of A with the Higgs to cancel against the loop-level contributions, which introduces an additional fine-tuning in the scalar sector. The $\mathrm{SU}(2)_\ell$ gauge bosons $W'_{1,2}$ and Z'_ℓ also develop ∼100 EeV masses. We do not provide detailed formulas here, since for the case of $\mathrm{SU}(2)_\ell$ breaking we are interested only in the gravitational wave signal from domain walls, which is determined solely by the vacuum expectation value v_Ψ and the $\mathcal{Z}_2$ symmetry breaking parameter m_{12}^2.

The masses of the gauge bosons G' and Z' arising from SU(4) symmetry breaking are

$$\begin{aligned} m_{G'} &= \frac{1}{2} g_4 v_\Phi, \\ m_{Z'} &= \frac{1}{2}\sqrt{\frac{3}{2} g_4^2 + g_X^2}\, v_\Phi, \end{aligned} \tag{13}$$

while the mass of the radial mode of the scalar $\hat{\Phi}$ is

$$m_\Phi = \sqrt{2\lambda_\Phi} v_\Phi. \tag{14}$$

Since the SU(4) symmetry is broken down to $\mathrm{SU}(3)_c$, the gauge coupling g_4 needs to match the strong coupling g_s at the symmetry breaking scale. To determine the corresponding value, we run g_s via the renormalization group equation

$$\frac{\partial g_s(\mu)}{\partial \log \mu} = -\frac{7 g_s^3(\mu)}{16\pi^2}. \tag{15}$$

For instance, this gives $g_4(100\ \text{TeV}) \simeq 0.88$. The value of g_X at that scale is then fixed by the relation [15]

$$g_X = \frac{g_4 g_Y}{\sqrt{g_4^2 - \frac{2}{3} g_Y^2}}, \tag{16}$$

where g_Y is the weak hypercharge coupling at that scale, which leads to $g_X(100\ \text{TeV}) \simeq 0.30$.

D. Nonperturbative interactions

At energies above the $\mathrm{SU}(2)_\ell$ breaking scale the model exhibits nonperturbative dynamics generated by $\mathrm{SU}(2)_\ell$ instantons [16]. Those instantons induce dimension-six interactions of the following form:

$$\begin{aligned}\mathcal{O} \sim \epsilon_{ij}[&(l_L^i \cdot \bar{\nu}_R)(l_L^j \cdot \bar{e}_R) - (\tilde{l}_L^i \cdot \bar{\tilde{\nu}}_R)(l_L^j \cdot \bar{e}_R) \\ &+ (l_L^i \cdot \tilde{l}_L^j)(\bar{\nu}_R \cdot \bar{\tilde{e}}_R) - (l_L^i \cdot \tilde{l}_L^j)(\bar{\tilde{\nu}}_R \cdot \bar{e}_R) \\ &+ (\tilde{l}_L^i \cdot \bar{\tilde{\nu}}_R)(\tilde{l}_L^j \cdot \bar{\tilde{e}}_R) - (l_L^i \cdot \bar{\nu}_R)(\tilde{l}_L^j \cdot \bar{\tilde{e}}_R)],\end{aligned} \tag{17}$$

where the dot represents Lorentz contraction and there is an implicit sum over the family indices. Those nonperturbative processes violate the otherwise accidentally conserved Standard Model lepton number.

Indeed, the Lagrangian in Eq. (11) possesses two exact global U(1) symmetries and one approximate global U(1) symmetry in the limit of small neutrino Yukawas $y_\nu, y'_\nu \ll 1$ (see [16] for concrete charge assignments). It is convenient to construct linear combinations of those symmetries corresponding to the generalized lepton number and dark matter number. Upon symmetry breaking, the only fields charged under the dark matter global U(1) and neutral under the generalized lepton number U(1) are ν_R, $\tilde{\nu}_R$, and ν'_L. Whenever an odd number of them is involved in a process, those global U(1) symmetries are broken.

For example, the second term in Eq. (17) leads to the instanton-induced process

$$\nu_L \tilde{e}_L \to \tilde{\nu}_R e_R, \tag{18}$$

which violates the conventional lepton number, $\Delta L = -1$, and the dark matter number, $\Delta\chi = 1$, since out of the four fields participating in this interaction only $\tilde{\nu}_R$ does not carry the lepton number, and it is also the only field carrying the dark matter number. This field is the right-handed component of one of the two dark matter candidates in the model.

III. DARK MATTER

There are two particles which are singlets under all gauge groups of the theory—we denote them by $\tilde{\nu}'_1$ and $\tilde{u}'_1$. They correspond to the following left- and right-handed components of the fields existing before symmetry breaking:

$$\begin{aligned} \tilde{\nu}'_1 &: \ (\tilde{\nu}'_1)_L \approx \nu'^1_L, \qquad (\tilde{\nu}'_1)_R \approx \tilde{\nu}^1_R, \\ \tilde{u}'_1 &: \ (\tilde{u}'_1)_L \approx u'^1_L, \qquad (\tilde{u}'_1)_R \approx \tilde{u}^1_R, \end{aligned} \tag{19}$$

where we assumed that the dark matter belongs to the first generation of the extra fermions, which is an arbitrary choice.

The particle $\tilde{\nu}'_1$ is one of the 12 fermionic states which arise after $SU(2)_\ell$ breaking and develop vectorlike masses through the vacuum expectation values of $\hat{\Psi}_1$ and $\hat{\Psi}_2$. Due to the conservation of a remnant U(1) global symmetry [16], under which the new fields transform as

$$\begin{aligned} &\tilde{l}_L \to e^{i\phi}\tilde{l}_L, \qquad \tilde{e}_R \to e^{i\phi}\tilde{e}_R, \qquad \tilde{\nu}_R \to e^{i\phi}\tilde{\nu}_R, \\ &l'_R \to e^{i\phi} l'_R, \qquad e'_L \to e^{i\phi} e'_L, \qquad \nu'_L \to e^{i\phi}\nu'_L, \end{aligned} \tag{20}$$

those fermions cannot decay exclusively to Standard Model particles. Therefore, the lightest of them remains stable and, if it is also electrically neutral, such as $\tilde{\nu}'_1$, it becomes a good dark matter candidate. The Yukawa matrices can be chosen such that the nondark matter fermions are heavy, whereas $\tilde{\nu}'_1$ is light. As demonstrated in [16], the dark matter annihilation channel to lighter CP-odd scalars A (see Fig. 1),

$$\tilde{\nu}'_1 \bar{\tilde{\nu}}'_1 \to AA, \tag{21}$$

is sufficiently efficient to remove the symmetric component of dark matter. The remaining asymmetric component

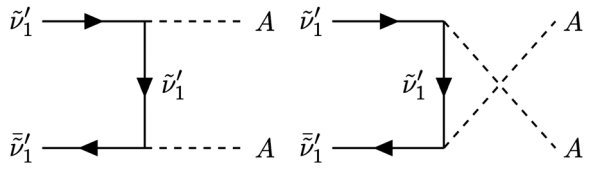

FIG. 1. Annihilation channels for the dark matter particle $\tilde{\nu}'_1$.

contributes to the observed dark matter relic abundance, as will be discussed in Sec. IV.

The breaking of the SU(4) symmetry also results in 12 fermionic states with vectorlike masses, this time generated by the vacuum expectation value of $\hat{\Phi}$. Once again, because of the conservation of an accidental global U(1) symmetry [15], under which the Standard Model quark partners transform as

$$\begin{aligned} &\tilde{Q}_L \to e^{i\theta}\tilde{Q}_L, \qquad \tilde{u}_R \to e^{i\theta}\tilde{u}_R, \qquad \tilde{d}_R \to e^{i\theta}\tilde{d}_R, \\ &Q'_R \to e^{i\theta} Q'_R, \qquad u'_L \to e^{i\theta} u'_L, \qquad d'_L \to e^{i\theta} d'_L, \end{aligned} \tag{22}$$

their decay channels cannot involve solely Standard Model particles in the final state. If the lightest of them is the electrically neutral $\tilde{u}'_1$, it remains stable and becomes another viable component of dark matter. The dark matter annihilation leading to the correct relic abundance happens through the t-channel and u-channel processes $\tilde{u}'_1\bar{\tilde{u}}'_1 \to \psi\psi$, where ψ is an additional light scalar particle coupled to the dark matter via $\mathcal{L}_\psi = g\psi\bar{\tilde{u}}'_1\tilde{u}'_1$, and in this case a successful asymmetric dark matter scenario can also be realized [15].

It is worth emphasizing that with two asymmetric dark matter candidates, their individual masses are not fixed by a single relic density requirement. Depending on the contribution of each of them to the relic abundance, one of them can have a mass smaller than the mass of the neutron, possibly introducing a connection to the dark matter models relevant for the neutron lifetime anomaly [100].

IV. MATTER-ANTIMATTER ASYMMETRY

The generation of a matter-antimatter imbalance in the model proceeds via two independent processes: leptogenesis and baryogenesis, both occurring in an asymmetric dark matter setting [17–22]. Leptogenesis, as demonstrated in [16], is realized through instantons during $SU(2)_\ell$ breaking, whereas baryogenesis, as argued in [15], is achieved within the SU(4) sector through the effects of higher-dimensional operators. We discuss both mechanisms below.

The complete formula for the effective potential generated by $\hat{\Psi}_1$ and $\hat{\Psi}_2$ was derived in [69], where it was demonstrated that a first order phase transition from $SU(2)_\ell$ breaking can occur. This scenario is realized in the model considered in this work, but happens at a higher symmetry breaking scale. Figure 2 shows a plot of the effective potential $V_{\rm eff}(\psi_1, \psi_2, T)$ produced using *Mathematica* [101], assuming the parameters $\lambda_i = 0.001$, $v_1 = v_2$, $v_\Psi = 100$ EeV, $g_\ell = 1$, at high temperature (red) and at low temperature (green). As the temperature drops, the potential develops new vacua with lower energy densities (see [69] for details), separated by a barrier from the high-temperature vacuum. This leads to a first order phase transition, which is precisely the out-of-equilibrium condition enabling leptogenesis to happen, and combines the framework of asymmetric dark

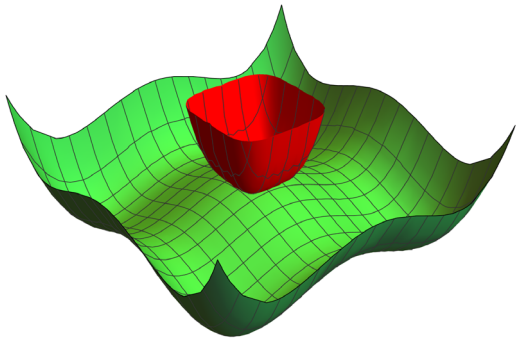

FIG. 2. Effective potential of the model $V_{\rm eff}(\psi_1,\psi_2,T)$ at low temperature (green) and high temperature (red).

matter with several other leptogenesis/baryogenesis mechanisms [102–105].

There are four vacua of this type for the scalar potential $V_{\rm eff}(\psi_1,\psi_2)$, but since two of them are related through the gauge transformation $\Psi_i \to e^{i\theta}\Psi_i$, only two of the four vacua are physically distinct [106,107]. We denote them by $\vec{\psi}_{\rm vac1}$ and $\vec{\psi}_{\rm vac2}$. The degeneracy between the energy densities of these vacua is broken by the $\mathcal{Z}_2$ symmetry breaking terms in the effective potential, primarily governed by the parameter m_{12}^2.

The first order phase transition corresponds to the nucleation of bubbles with a true vacuum inside. Outside the bubble the nonperturbative $\mathrm{SU}(2)_\ell$ instanton-induced processes described by Eq. (17) remain active. This, along with a sufficiently large amount of CP violation (provided by the appropriate terms in the scalar potential for $\hat{\Psi}_1$ and $\hat{\Psi}_2$), leads to the generation of a lepton number excess. As the bubble expands, those regions get trapped inside the bubble, where lepton number violation no longer occurs, leading to the accumulation of the lepton number in the Universe. Since the instantons also violate the global dark matter U(1) symmetry (as discussed in Sec. II), this results in the generation of a dark matter asymmetry as well. This process is described by a set of 12 diffusion equations, which have the general form [108,109]

$$\frac{\partial \rho_{Ni}}{\partial t} = D_i \nabla^2 \rho_{Ni} - \sum_j \Gamma_{ij}\frac{\rho_{Nj}}{n_j} + \gamma_i. \tag{23}$$

In the expression above, ρ_{Ni} is the particle number density, D_i and Γ_{ij} are the diffusion constant and rate, respectively, n_j is the number of degrees of freedom, and γ_i is the ith CP-violating source given by [110]

$$\gamma_i \approx \frac{\lambda_7 \mu_{12}^2}{32\pi}\frac{\Gamma_{\psi_i} T_*}{m_{\psi_i}^3(T_*)}\partial_z \psi_i, \tag{24}$$

where T_* is the bubble nucleation temperature, Γ_{ψ_i} is the decay rate of ψ_i, the z-axis is in the direction perpendicular to the bubble wall, and $\mu_{12}^2 = \mathrm{Re}(m_{12}^2)$. Solving the diffusion equations for our set of parameters reveals that the generated lepton asymmetry versus the dark matter asymmetry is

$$\frac{|\Delta L|}{|\Delta \tilde{\nu}_1'|} = 3, \tag{25}$$

consistent with the existing result [16]. The amount of lepton asymmetry produced in this process is subsequently altered by the electroweak sphalerons [111], which partially convert it into a baryon asymmetry,

$$|\Delta B| = \frac{84}{79}|\Delta \tilde{\nu}_1'|. \tag{26}$$

Assuming a bubble wall velocity equal to the speed of light, we find that for $v_\Psi = 100$ EeV and $\lambda_i \sim 10^{-4}$ the observed baryon-to-photon ratio [112]

$$\eta \sim 6 \times 10^{-10} \tag{27}$$

is generated provided that

$$|\lambda_7 \mu_{12}^2| Y^2 \sim 10^{-10}\ \mathrm{EeV}^2. \tag{28}$$

This condition can be satisfied by a wide range of parameter values, e.g., $\lambda_7 \sim 10^{-6}$, $\mu_{12}^2 \sim 10^{-2}$ EeV^2, and $Y \sim 10^{-1}$ (in the case $v_\Psi = 100$ EeV). The dark matter mass is then given by

$$m_{\tilde{\nu}_1'} \approx \frac{\Omega_{\tilde{\nu}_1'}}{\Omega_B}\frac{|\Delta B|}{|\Delta \tilde{\nu}_1'|} m_{\rm proton}. \tag{29}$$

If the $\tilde{\nu}_1'$ particle makes up all of the dark matter in the Universe, this condition implies $m_{\tilde{\nu}_1'} \approx 5$ GeV. However, $\tilde{\nu}_1'$ can be lighter if the dark matter in the Universe consists also of the $\tilde{u}_1'$ particles.

Indeed, an analogous asymmetric dark matter mechanism can generate a contribution to the baryon and dark matter asymmetries in the SU(4) sector. As pointed out in [15], the following dimension-six operators,

$$\frac{c_1}{\Lambda^2}\epsilon_{abcd}\hat{u}_R^a \hat{u}_R^b \hat{d}_R^c \hat{d}_R^d, \qquad \frac{c_2}{\Lambda^2}\epsilon_{abcd}(\hat{Q}_L^a \epsilon \hat{Q}_L^b)(\hat{Q}_L^c \epsilon \hat{Q}_L^d), \tag{30}$$

violate baryon and dark matter numbers by one unit, and the initially produced asymmetries are related via $\Delta B_i = -\Delta \tilde{u}_1'$. The baryon asymmetry is then depleted because of the effect of electroweak sphalerons to

$$|\Delta B| = \frac{28}{79}|\Delta \tilde{u}_1'|. \tag{31}$$

The mass of the $\tilde{u}_1'$ particle in such an asymmetric dark matter scenario is

$$m_{\tilde{u}'_1} \approx \frac{\Omega_{\tilde{u}'_1}}{\Omega_B}\frac{|\Delta B|}{|\Delta \tilde{u}'_1|} m_{\text{proton}}. \tag{32}$$

If all of the dark matter consists of the $\tilde{u}'_1$ particles, then their mass is $m_{\tilde{u}'_1} \approx 1.75$ GeV. However, similarly as before, this mass can be smaller if the $\tilde{\nu}'_1$ particles also contribute.

With two dark matter candidates, the dark matter relic abundance is given by the sum of the two contributions

$$\Omega_{\text{DM}} = \varepsilon\, \Omega_{\tilde{\nu}'_1} + (1-\varepsilon)\, \Omega_{\tilde{u}'_1}, \tag{33}$$

where ε can take any value between 0 and 1. Given the relations in Eqs. (29) and (32), one of the particles $\tilde{\nu}'_1$ and $\tilde{u}'_1$ can have a mass smaller than that of the neutron, introducing a possible connection to models proposed to explain the neutron lifetime puzzle [100].

V. DOMAIN WALL SIGNATURES

When the $\text{SU}(2)_\ell$ symmetry is spontaneously broken, patches of the Universe undergo a first order phase transition to one of the vacua described earlier: $\vec{\psi}_{\text{vac1}}$ or $\vec{\psi}_{\text{vac2}}$. Since those two vacua correspond to disconnected manifolds, domain walls are created along their boundaries. The breaking of the $\mathcal{Z}_2$ symmetry between the vacua is essential, since without it domain walls would remain stable, leading to cosmological problems, as they would result in unacceptably large density fluctuations in the Universe [51].

In our model the $\mathcal{Z}_2$ symmetry is softly broken by the small m_{12}^2 term, so that the vacua $\vec{\psi}_{\text{vac1}}$ and $\vec{\psi}_{\text{vac2}}$ have slightly different energy densities. This introduces an instability of the created domain walls and leads to their annihilation, which in turn gives rise to a stochastic gravitational wave background. It is worth noting that for domain walls to actually form, the $\mathcal{Z}_2$ symmetry can only be softly broken; otherwise, patches of the Universe would predominantly tunnel to the lower energy density state and no topological defects would arise.

A. Domain wall creation and annihilation

Choosing the z-axis to be perpendicular to the domain wall, the profile of the static configuration $\vec{\psi}_{dw}(z)$ is given by the solution of the equation

$$\frac{d^2\vec{\psi}_{dw}(z)}{dz^2} - \vec{\nabla}_\psi V_{\text{eff}}[\vec{\psi}_{dw}(z)] = 0, \tag{34}$$

subject to the boundary conditions

$$\vec{\psi}_{dw}(z=-\infty) = \vec{\psi}_{\text{vac1}}, \qquad \vec{\psi}_{dw}(z=\infty) = \vec{\psi}_{\text{vac2}}. \tag{35}$$

One of the domain wall parameters, which the resulting gravitational wave signal depends on, is the tension σ,

$$\sigma = \int_{-\infty}^{\infty} dz\, \rho_{dw}(z), \tag{36}$$

where ρ_{dw} is the energy density of the domain wall,

$$\rho_{dw}(z) = \frac{1}{2}\left(\frac{d\vec{\psi}_{dw}(z)}{dz}\right)^2 + V_{\text{eff}}[\vec{\psi}_{dw}(z)]. \tag{37}$$

In our case the tension can be estimated as

$$\sigma \sim v_\Psi^3. \tag{38}$$

The second parameter governing the gravitational wave spectrum is the difference between the energy densities of the two vacua $\Delta\rho$ (also called the potential bias), which in our model can be approximated by

$$\Delta\rho \sim \mu_{12}^2 v_\Psi^2. \tag{39}$$

If the potential bias is nonzero, the domain walls become unstable and annihilate when the volume pressure, $p_V \sim \Delta\rho$, exceeds the pressure due to tension, $p_T \sim \sigma^2/M_{\text{Pl}}^2$, where M_{Pl} is the Planck mass. This implies the following condition on the parameters of our model:

$$\mu_{12}^2 \gtrsim \frac{v_\Psi^4}{M_{\text{Pl}}^2}. \tag{40}$$

For example, if $v_\Psi \sim 100$ EeV, then for the domain walls to annihilate promptly one requires $\mu_{12}^2 \gtrsim 1$ TeV^2, whereas for $v_\Psi \sim 1$ EeV this bound is relaxed to 10^{-2} GeV^2. The additional constraint on μ_{12}^2 assuring that domain wall annihilation happens before big bang nucleosynthesis (so that it does not alter the ratios of the produced elements) is much weaker.

B. Gravitational wave signal

The annihilation of domain walls gives rise to a stochastic gravitational wave background described by [39,51]

$$h^2\Omega_{\text{DW}}(\nu) \approx 7\times 10^{-21}\left(\frac{g_*}{100}\right)^{-\frac{1}{3}}\left(\frac{\sigma}{\text{EeV}^3}\right)^4\left(\frac{\text{PeV}^4}{\Delta\rho}\right)^2 \times\left[\left(\frac{\nu}{\nu_d}\right)^3\theta(\nu_d-\nu)+\left(\frac{\nu_d}{\nu}\right)\theta(\nu-\nu_d)\right], \tag{41}$$

where we adopted the values of the area parameter $\mathcal{A}=0.8$ and efficiency parameter $\tilde{\epsilon}_{\text{gw}}=0.7$ [113], g_* is the number of degrees of freedom, $\theta(x)$ is the Heaviside step function, and ν_d is the peak frequency given by

$$\nu_d \approx (4.5\text{ Hz})\sqrt{\frac{\text{EeV}^3}{\sigma}\frac{\Delta\rho}{\text{PeV}^4}}. \tag{42}$$

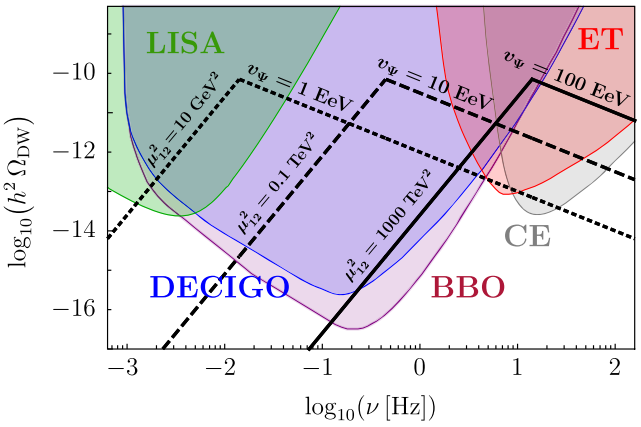

FIG. 3. Gravitational wave signals from domain wall annihilation for several choices of parameters. The colored regions correspond to the reach of future gravitational wave experiments: LISA (green), Big Bang Observer (purple), DECIGO (blue), Einstein Telescope (red), and Cosmic Explorer (gray).

As described by Eq. (41), the spectrum scales as $\sim\nu^3$ for frequencies below the peak frequency and $\sim 1/\nu$ for higher frequencies. The constraints arising from the cosmic microwave background measurements impose the condition $h^2\Omega(\nu) < 2.9 \times 10^{-7}$ [114], which requires the parameters v_Ψ and μ_{12}^2 in our model to satisfy the relation

$$\frac{v_\Psi^4}{\mu_{12}^2} \lesssim (2.5 \times 10^9\ \text{EeV})^2. \tag{43}$$

Figure 3 shows the expected gravitational wave signal from domain walls for several choices of model parameters, plotted over the sensitivity regions of future gravitational wave detectors: LISA [24], BBO [25], DECIGO [26], ET [27], and CE [28]. Figure 4 displays regions of parameter space for which the signal can be detected at those

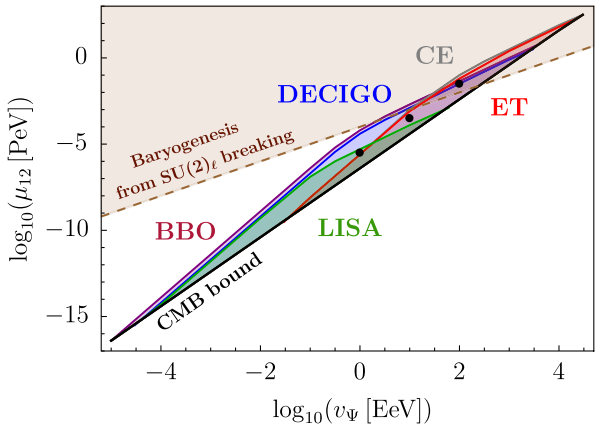

FIG. 4. Parameter space regions where the gravitational wave signal from domain walls has a signal-to-noise ratio of at least five after one year of collecting data for various experiments. The black dots correspond to the three signatures shown in Fig. 3.

experiments—the upper bound on μ_{12} is detector-specific (the colors correspond to the selection made in Fig. 3), whereas the lower bound arises from the cosmic microwave background radiation constraint in Eq. (43).

We note that among the three gravitational wave signatures in Fig. 3, only the rightmost curve corresponds to a choice of parameters for which the matter-antimatter asymmetry of the Universe can be generated entirely through $SU(2)_\ell$ breaking. Figure 4 shows the full parameter space corresponding to this case (brown-shaded region). The dashed line was determined by using the fact that the right-hand side of Eq. (28) scales as v_Ψ^2, and by setting the dimensionless couplings to one. For the other two curves in Fig. 3 and the remaining parameter space in Fig. 4, a portion of the baryon asymmetry needs to be generated by SU(4) breaking.

VI. PHASE TRANSITION SIGNATURES

We consider now the possibility of having a first order phase transition associated with SU(4) breaking occurring at the PeV scale and producing a measurable gravitational wave signal. We first calculate the effective potential of the model. We then proceed to compute the parameters governing the dynamics of the bubble nucleation, and ultimately determine the shape of the possible gravitational wave signatures.

A. Effective potential

Denoting the background field by ϕ, the three contributions to the effective potential are the tree-level term $V_0(\phi)$, the Coleman-Weinberg one-loop correction $V_{\rm CW}(\phi)$, and the finite temperature part $V_T(\phi, T)$, so that

$$V_{\rm eff}(\phi, T) = V_0(\phi) + V_{\rm CW}(\phi) + V_T(\phi, T). \tag{44}$$

Substituting in Eq. (6) the value of m_Φ^2 obtained from minimizing the potential, one obtains

$$V_0(\phi) = -\frac{1}{2}\lambda_\Phi v_\Phi^2 \phi^2 + \frac{1}{4}\lambda_\Phi \phi^4. \tag{45}$$

For the Coleman-Weinberg contribution, we use the cutoff regularization scheme and set the minimum of the zero temperature potential and the mass of ϕ to be equal to their tree-level values, which results in [115]

$$V_{\rm CW}(\phi) = \sum_i \frac{n_i}{(8\pi)^2}\left\{ m_i^4(\phi)\left[\log\left(\frac{m_i^2(\phi)}{m_i^2(v_\Phi)}\right) - \frac{3}{2}\right] + 2m_i^2(\phi)m_i^2(v_\Phi)\right\}, \tag{46}$$

where contributions from all particles charged under SU(4) are summed over, including χ (the Goldstone bosons), n_i is the number of degrees of freedom, and m_i are the background

field-dependent masses [we substitute $m_\chi(v) \to m_\Phi(v)$ for the Goldstone bosons, where Φ is the radial mode]. Those masses for the gauge bosons are

$$m_{G'}(\phi) = \frac{1}{2} g_4 \phi,$$
$$m_{Z'}(\phi) = \frac{1}{2}\sqrt{\frac{3}{2} g_4^2 + g_X^2}\,\phi, \tag{47}$$

and for the radial mode of the scalar $\hat{\Phi}$,

$$m_\Phi = \sqrt{2\lambda_\Phi}\,\phi. \tag{48}$$

The corresponding numbers of degrees of freedom are $n_{G'} = 18$, $n_{Z'} = 3$, $n_\Phi = 1$, and $n_\chi = 7$.

Finally, the finite temperature part of the effective potential is given by [116]

$$V_T(\phi, T) = \frac{T^4}{2\pi^2}\sum_i n_i \int_0^\infty dx\, x^2 \log\left[1 \mp e^{-\sqrt{x^2 + \frac{m_i^2(\phi)}{T^2}}}\right] + \frac{T}{12\pi}\sum_k n'_k \{m_k^3(\phi) - [m_k^2(\phi) + \Pi_k(T)]^{3/2}\}, \tag{49}$$

where the first line is generated by one-loop diagrams (the sum is over all particles), while the second line arises from the daisy diagrams (the sum is over bosons only). The prime symbol indicates that only longitudinal degrees of freedom in the case of vector bosons are included (i.e., $n'_{G'} = 6$, $n'_{Z'} = 1$, $n'_\Phi = 1$, $n'_\chi = 7$), and $\Pi_k(T)$ are the thermal masses [117], which in our model are calculated to be (for $\lambda_\Phi \ll 1$)

$$\Pi_{G'}(T) = \Pi_{Z'}(T) = \frac{8}{3} g_4^2 T^2,$$
$$\Pi_\Phi(T) = \Pi_\chi(T) = \frac{1}{16}\left(g_X^2 + \frac{15}{2} g_4^2\right) T^2. \tag{50}$$

Figure 5 shows the resulting effective potential plotted adopting $v_\Phi = 100$ TeV, the values of g_4 and g_X at that scale (as discussed in Sec. II C), and $\lambda_\Phi = 0.004$ [given Eqs. (11)–(14), for this choice of parameters all new particles, including the scalar Φ, are beyond the reach of the Large Hadron Collider]. With decreasing temperature, a new true vacuum is formed with a lower energy density than the high temperature false vacuum. Since there is a potential barrier between the two minima, a first order phase transition becomes possible.

B. Bubble nucleation

When the temperature drops below the so-called nucleation temperature T_*, this initiates the transition of various

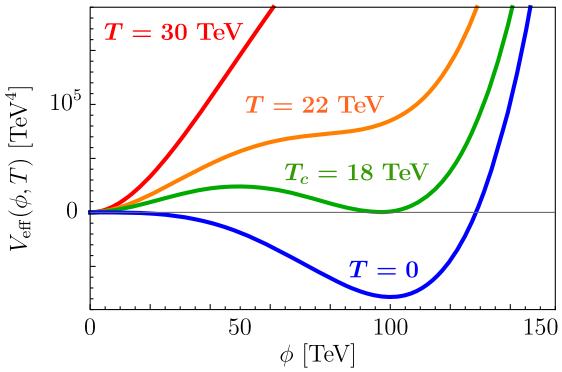

FIG. 5. Effective potential of the SU(4) sector of the model, $V_{\rm eff}(\phi, T)$, assuming $v_\Phi = 100$ TeV and $\lambda_\Phi = 0.004$, for several choices of temperature.

parts of the Universe from the false vacuum to the true one. Such first order phase transitions correspond to the nucleation of bubbles of a true vacuum. The nucleation temperature can be determined from the condition that the bubble nucleation rate $\Gamma(T)$ becomes comparable to the Hubble expansion rate,

$$\Gamma(T_*) \sim H(T_*)^4. \tag{51}$$

The nucleation rate is given by [118]

$$\Gamma(T) \approx \left(\frac{S(T)}{2\pi T}\right)^{\frac{3}{2}} T^4 e^{-S(T)/T}, \tag{52}$$

in which $S(T)$ is the Euclidean action calculated as

$$S(T) = 4\pi \int dr\, r^2 \left[\frac{1}{2}\left(\frac{d\phi_b}{dr}\right)^2 + V_{\rm eff}(\phi_b, T)\right], \tag{53}$$

where $\phi_b(r)$ is the bounce solution describing the profile of the expanding bubble, i.e., the solution to the equation

$$\frac{d^2\phi}{dr^2} + \frac{2}{r}\frac{d\phi}{dr} - \frac{d}{d\phi} V_{\rm eff}(\phi, T) = 0, \tag{54}$$

subject to the following boundary conditions:

$$\left.\frac{d\phi}{dr}\right|_{r=0} = 0, \qquad \phi(\infty) = \phi_{\rm false}. \tag{55}$$

The nucleation temperature is calculated, using Eqs. (51) and (52), as the solution to the equation

$$\frac{S(T_*)}{T_*} \approx 4 \log\left[\frac{M_{\rm Pl}}{T_*}\right] - 2 \log\left[\frac{4\pi^3 g_*}{45}\left(\frac{2\pi T_*}{S(T_*)}\right)^{\frac{3}{4}}\right]. \tag{56}$$

C. Gravitational wave signal

During the nucleation and the violent expansion of bubbles of a true vacuum, a stochastic gravitational wave background is generated via bubble wall collisions, sound shock waves in the primordial plasma, and magnetohydrodynamic turbulence. The shape of the spectrum is determined through simulations and depends only on four quantities: bubble wall velocity v_w (assumed here to be equal to the speed of light; see [119,120] for more details), nucleation temperature T_*, strength of the phase transition α, and duration of the phase transition $1/\tilde{\beta}$. Those parameters depend on the shape of the effective potential, which itself is specific to the particular particle physics model under investigation. This introduces a correspondence between the fundamental parameters of the Lagrangian and the resulting gravitational wave signal.

Upon determining the nucleation temperature T_* by solving Eq. (56), the parameter α is calculated as

$$\alpha = \frac{\rho_{\rm vac}(T_*)}{\rho_{\rm rad}(T_*)}, \tag{57}$$

i.e., as the ratio of the difference between the energy densities of the true and false vacua,

$$\rho_{\rm vac}(T) = V_{\rm eff}(\phi_{\rm false}, T) - V_{\rm eff}(\phi_{\rm true}, T) - T\frac{\partial}{\partial T}[V_{\rm eff}(\phi_{\rm false}, T) - V_{\rm eff}(\phi_{\rm true}, T)], \tag{58}$$

and the radiation energy density

$$\rho_{\rm rad}(T) = \frac{\pi^2}{30} g_* T^4. \tag{59}$$

The parameter $\tilde{\beta}$ is computed as

$$\tilde{\beta} = T_* \frac{d}{dT}\left[\frac{S(T)}{T}\right]\Big|_{T=T_*}. \tag{60}$$

Based on numerical simulations, the contribution to the stochastic gravitational wave spectrum from sound waves is given by the empirical formula [120,121]

$$h^2\Omega_{\rm sound}(\nu) \approx \frac{1.9\times 10^{-5}}{\tilde{\beta}}\left(\frac{g_*}{100}\right)^{-\frac{1}{3}}\left(\frac{\alpha\kappa_s}{\alpha+1}\right)^2 \times \frac{(\nu/\nu_s)^3}{[1+0.75(\nu/\nu_s)^2]^{\frac{7}{2}}}\Upsilon, \tag{61}$$

where the fraction of the latent heat transformed into the bulk motion of the plasma [119] and the peak frequency are

$$\kappa_s = \frac{\alpha}{0.73 + 0.083\sqrt{\alpha} + \alpha}, \qquad \nu_s = (0.019\ {\rm Hz})\left(\frac{T_*}{100\ {\rm TeV}}\right)\left(\frac{g_*}{100}\right)^{\frac{1}{6}}\tilde{\beta}, \tag{62}$$

and the suppression factor is given by [122,123]

$$\Upsilon = 1 - \frac{1}{\sqrt{1 + \frac{8\pi^{1/3}}{\tilde{\beta}}\sqrt{\frac{\alpha+1}{3\alpha\kappa_s}}}}. \tag{63}$$

The gravitational wave spectrum contribution from bubble wall collisions is estimated to be [29,120,124] (see [125] for recent updates)

$$h^2\Omega_{\rm collision}(\nu) \approx \frac{4.9\times 10^{-6}}{\tilde{\beta}^2}\left(\frac{\alpha\kappa_c}{\alpha+1}\right)^2\left(\frac{g_*}{100}\right)^{-\frac{1}{3}} \times \frac{(\nu/\nu_c)^{2.8}}{1+2.8(\nu/\nu_c)^{3.8}}, \tag{64}$$

where the fraction of the latent heat deposited into the bubble front [126] and the peak frequency are

$$\kappa_c = \frac{\frac{4}{27}\sqrt{\frac{3}{2}\alpha} + 0.72\alpha}{1 + 0.72\alpha}, \qquad \nu_c = (0.0037\ {\rm Hz})\left(\frac{T_*}{100\ {\rm TeV}}\right)\left(\frac{g_*}{100}\right)^{\frac{1}{6}}\tilde{\beta}. \tag{65}$$

Finally, magnetohydrodynamic turbulence adds the following contribution [127,128]:

$$h^2\Omega_{\rm turb}(\nu) \approx \frac{3.4\times 10^{-4}}{\tilde{\beta}}\left(\frac{\alpha\epsilon\kappa_s}{\alpha+1}\right)^{\frac{3}{2}}\left(\frac{g_*}{100}\right)^{-\frac{1}{3}} \times \frac{(\nu/\nu_t)^3}{(1+8\pi\nu/\nu_*)(1+\nu/\nu_t)^{11/3}}, \tag{66}$$

where the turbulence suppression parameter $\epsilon = 0.05$ [120], the peak frequency is

$$\nu_t = (0.027\ {\rm Hz})\left(\frac{T_*}{100\ {\rm TeV}}\right)\left(\frac{g_*}{100}\right)^{\frac{1}{6}}\tilde{\beta}, \tag{67}$$

and the parameter ν_* [120] is given by

$$\nu_* = (0.017\ {\rm Hz})\left(\frac{T_*}{100\ {\rm TeV}}\right)\left(\frac{g_*}{100}\right)^{\frac{1}{6}}. \tag{68}$$

The three contributions add up linearly, resulting in

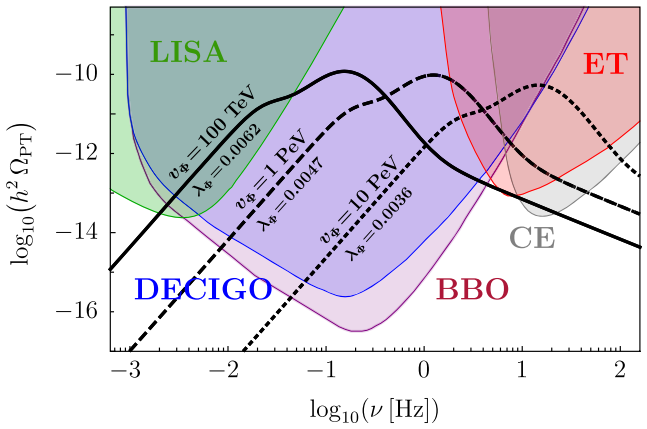

FIG. 6. Gravitational wave signals from a first order phase transition for several choices of parameters. The colored regions correspond to the reach of future gravitational wave experiments, as in Fig. 3.

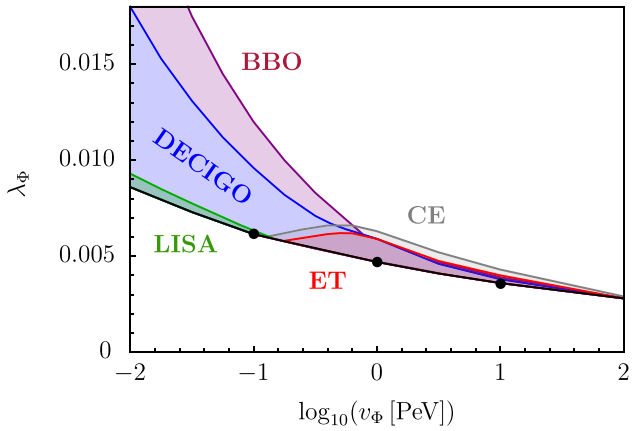

FIG. 7. Parameter space regions where the gravitational wave signal from a first order phase transition has a signal-to-noise ratio of at least five after one year of collecting data for various experiments. The black dots correspond to the three signatures shown in Fig. 6.

$$h^2\Omega_{\rm PT} = h^2\Omega_{\rm sound} + h^2\Omega_{\rm collision} + h^2\Omega_{\rm turb}. \quad (69)$$

Figure 6 illustrates the gravitational wave signatures of the model arising from a first order phase transition in the early universe for three different SU(4) symmetry breaking scales: $v_\Phi = 100$ TeV (solid line), 1 PeV (dashed line), and 10 PeV (dotted line), plotted for the quartic couplings λ_Φ which amplify the signal. In all of these cases the three contributions to the gravitational wave spectrum are visible: sound shock wave (main peak), bubble collision (to the left of the peak frequency), and magnetohydrodynamic turbulence (to the right of the peak). This is the result of the suppression factor Υ in Eq. (61), which reduces the contribution from sound waves roughly by a factor of 100—without this suppression the gravitational wave signal would be dominated entirely by the sound wave component.

The translation between the fundamental Lagrangian parameters $(v_\Phi, \lambda_\Phi, g_4, g_Y)$ and the phase transition parameters $(T_*, \alpha, \tilde{\beta})$ for each of the expected signals shown in Fig. 6 is provided in Table I. The gauge couplings g_4 and g_Y are fixed by the running of the Standard Model strong and electroweak couplings to have particular values at a given symmetry breaking scale, and thus the only free fundamental parameters are v_Φ and λ_Φ. The variation in the shape of the spectra shown in Fig. 6 arises precisely from the fact that the gauge couplings vary depending on the symmetry breaking scale—this affects the shape of the effective potential, and thus different values of the quartic coupling λ_Φ are required to amplify the signal.

TABLE I. Phase transition and fundamental Lagrangian parameters for the three gravitational wave signatures presented in Fig. 6.

Lagrangian parameters				Phase transition parameters		
v_Φ [TeV]	λ_Φ	g_4	g_X	α	$\tilde{\beta}$	T_* [TeV]
100	0.0062	0.88	0.30	9	220	3.2
1000	0.0047	0.82	0.29	30	260	22
10000	0.0036	0.77	0.29	43	350	190

Phase transitions corresponding to a higher symmetry breaking scale are characterized by a larger nucleation temperature, which shifts the signal toward higher frequencies. A shift in the same direction occurs for transitions described by a larger parameter $\tilde{\beta}$. The height of the peak is determined by both the strength of the phase transition α and its duration $1/\tilde{\beta}$: the signal is stronger for larger values of α and for smaller values of $\tilde{\beta}$ (longer phase transitions).

In addition to the signals themselves, the sensitivities of the future gravitational wave experiments LISA, DECIGO, BBO, ET, and CE are also shown in Fig. 6. To investigate in more detail how this reach translates into probing the fundamental parameters in the Lagrangian, we scanned over (v_Φ, λ_Φ) and determined the regions for which the above experiments will be sufficiently sensitive to detect the first order phase transition signals. The results of this scan are presented in Fig. 7.

VII. NEW GRAVITATIONAL WAVE SIGNATURE

An intriguing scenario arises when there is a large hierarchy between the $SU(2)_\ell$ and SU(4) symmetry breaking scales. This offers the possibility of having the domain wall signal and the first order phase transition signal coexist, both being within the sensitivity region of upcoming gravitational wave experiments, and producing novel, to us, features to search for in the gravitational wave spectrum.

To realize this unique signature, we assume that the $SU(2)_\ell$ symmetry is broken at the scale $v_\Psi \sim 100$ EeV, whereas the SU(4) is broken at $v_\Phi \sim 100$ TeV. The breaking

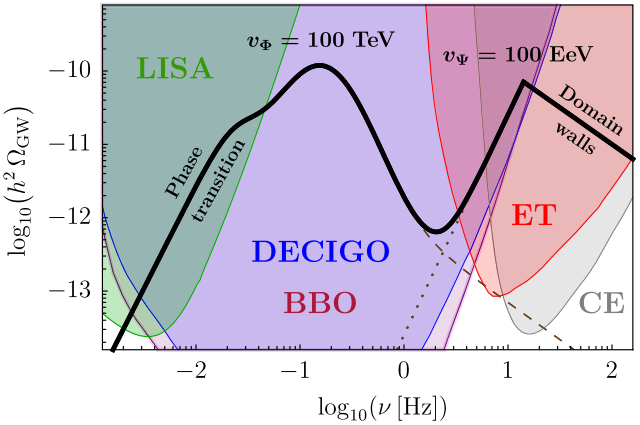

FIG. 8. Novel gravitational wave signature of the model expected when a large hierarchy between symmetry breaking scales exists. The signal is searchable in future gravitational wave detectors: LISA, DECIGO, BBO, ET, and CE.

of $SU(2)_\ell$ at the high scale leads to the production of domain walls, which undergo annihilation (due to the small nonzero μ_{12}^2 term) and produce a gravitational wave signal corresponding to the rightmost curve in Fig. 3. On the other hand, the SU(4) symmetry breaking at the lower scale results in a first order phase transition, which leads to a gravitational wave signal analogous to the leftmost curve in Fig. 6.

The two contributions combine to form a new double-bump gravitational wave signature shown in Fig. 8. The signal consists of a smooth peak arising from a first order phase transition and a second sharp peak corresponding to domain wall annihilation. The slopes for the two peaks are different and are described by the frequency power law behavior in Eqs. (41), (61), (64), and (66), which can be used to differentiate between the two contributions.

Another promising property of the signal is that it can be searched for throughout a wide range of frequencies, making it relevant for a number of upcoming gravitational wave experiments: LISA, DECIGO, BBO, ET, and CE. Moreover, several parts of the spectrum can be probed by more than one experiment, which would foster collaboration between the different groups in case of a future discovery.

We note, however, that the two symmetry breaking scales are not correlated with each other, and several other variations of the proposed signature are possible. For example, the order of the two peaks may be reversed, which happens if the $SU(2)_\ell$ is broken at $\sim$1 EeV while the SU(4) breaking occurs at $\sim$10 PeV. Another intriguing scenario is when the peak frequencies of the two bumps coincide [when $SU(2)_\ell$ is broken at $\sim$10 EeV and SU(4) is broken at $\sim$1 PeV], leading to an unusual dependence on frequency in the signal peak region. In general, if one requires the baryon asymmetry of the Universe to be generated solely by $SU(2)_\ell$ instantons, the symmetry breaking scale needs to be $v_\Psi \gtrsim 1$ EeV for the signal to be detectable in future gravitational wave experiments (one also needs the value of μ_{12} to lie in a specific range), as demonstrated in Fig. 4. On the other hand, the gravitational wave signal from a first order phase transition triggered by SU(4) breaking is within the reach of upcoming detectors if the symmetry breaking scale $v_\Phi \lesssim 100$ PeV (for appropriate values of λ_Φ), as shown in Fig. 7.

VIII. SUMMARY AND OUTLOOK

Physics beyond the Standard Model is certainly necessary to explain several outstanding questions such as: What is dark matter? How did the matter-antimatter asymmetry originate? How do neutrinos get their masses? In the time when conventional particle physics experiments, although working at the cutting edge of technological development and gathering extremely valuable data about the smallest and largest scales in the Universe, have not brought us answers to those questions, gravitational wave astronomy has provided us with a glimmer of hope to attack those problems from a new direction.

Processes taking place in the early universe and triggered by new physics, such as first order phase transitions, domain wall annihilation, or the dynamics of cosmic strings, can produce a stochastic gravitational wave background detectable in current and future experiments, offering us precious insight into the particle physics at the highest energies. This makes analyzing models leading to such gravitational wave signals a worthwhile endeavor.

In this paper, we propose a particle physics framework which enables answering the aforementioned open questions and gives rise to a unique gravitational wave signature. The new model contains two dark matter candidates and allows one to generate the matter-antimatter asymmetry of the Universe in an asymmetric dark matter setting through two distinct symmetry breaking events. Unlike in the case of typical asymmetric dark matter models, our scenario does not require the masses of the dark matter particles to be fixed at particular values. Depending on the individual contribution of each of them to the dark matter relic density, the mass of one of them can be below the mass of the neutron, opening up a possible connection to models explaining the neutron lifetime anomaly through a dark decay of the neutron [100].

The new signature consists of two peaks: one arising from a first order phase transition triggered by SU(4) symmetry breaking at $\sim$100 TeV, and the second one resulting from domain wall annihilation after $SU(2)_\ell$ breaking at $\sim$100 EeV. The signal spans a wide range of frequencies relevant for the upcoming gravitational wave experiments: LISA, DECIGO, BBO, ET, and CE. Since parts of the predicted signal lie in regions of overlapping sensitivities of various detectors, it also offers an opportunity of cross-checking the results, encouraging stronger collaboration within the gravitational wave physics community.

It would be interesting to investigate the possibility of an additional cosmic string contribution to the gravitational wave spectrum. Cosmic strings are typically produced when a U(1) gauge symmetry is spontaneously broken [34], and the resulting gravitational wave signal depends on the scale at which this happens [129,130]. However, it has recently been shown that cosmic strings can also be produced through the breaking of non-Abelian gauge symmetries. For example, if an SU(2) gauge group is broken by the vacuum expectation values of two triplet scalars (instead of the two doublets as in the model we considered), topologically stable strings can form [131,132]. The interplay between the cosmic string contribution and other gravitational wave signatures will be the subject of an upcoming publication [133].

A discovery of a stochastic gravitational wave background, such as the one discussed in this paper, would introduce a breakthrough in our understanding of the early universe, shedding light on what happened just a small fraction of a second after the big bang.

ACKNOWLEDGMENTS

We thank the *Physical Review D* referee for constructive comments regarding the manuscript. This research was supported by the National Science Foundation under Grant No. PHY-2213144.

[1] S. L. Glashow, Partial symmetries of weak interactions, Nucl. Phys. **22**, 579 (1961).
[2] P. W. Higgs, Broken Symmetries and the Masses of Gauge Bosons, Phys. Rev. Lett. **13**, 508 (1964).
[3] F. Englert and R. Brout, Broken Symmetry and the Mass of Gauge Vector Mesons, Phys. Rev. Lett. **13**, 321 (1964).
[4] S. Weinberg, A Model of Leptons, Phys. Rev. Lett. **19**, 1264 (1967).
[5] A. Salam, Weak and electromagnetic interactions, Conf. Proc. C **680519**, 367 (1968).
[6] H. Fritzsch, M. Gell-Mann, and H. Leutwyler, Advantages of the color octet gluon picture, Phys. Lett. **47B**, 365 (1973).
[7] D. J. Gross and F. Wilczek, Ultraviolet Behavior of Non-abelian Gauge Theories, Phys. Rev. Lett. **30**, 1343 (1973).
[8] H. D. Politzer, Reliable Perturbative Results for Strong Interactions?, Phys. Rev. Lett. **30**, 1346 (1973).
[9] S. Chatrchyan *et al.* (CMS Collaboration), Observation of a new boson at a mass of 125 GeV with the CMS experiment at the LHC, Phys. Lett. B **716**, 30 (2012).
[10] G. Aad *et al.* (ATLAS Collaboration), Observation of a new particle in the search for the standard model Higgs boson with the ATLAS detector at the LHC, Phys. Lett. B **716**, 1 (2012).
[11] V. C. Rubin and Jr. Ford, W. K., Rotation of the Andromeda Nebula from a spectroscopic survey of emission regions, Astrophys. J. **159**, 379 (1970).
[12] P. de Bernardis *et al.* (Boomerang Collaboration), A flat universe from high resolution maps of the cosmic microwave background radiation, Nature (London) **404**, 955 (2000).
[13] R. Gavazzi, T. Treu, J. D. Rhodes, L. V. Koopmans, A. S. Bolton, S. Burles, R. Massey, and L. A. Moustakas, The sloan lens ACS survey. 4. The mass density profile of early-type galaxies out to 100 effective radii, Astrophys. J. **667**, 176 (2007).
[14] J. L. Feng, Dark matter candidates from particle physics and methods of detection, Annu. Rev. Astron. Astrophys. **48**, 495 (2010).
[15] B. Fornal, A. Rajaraman, and T. M. P. Tait, Baryon number as the fourth color, Phys. Rev. D **92**, 055022 (2015).
[16] B. Fornal, Y. Shirman, T. M. P. Tait, and J. Rittenhouse West, Asymmetric dark matter and baryogenesis from $SU(2)_\ell$, Phys. Rev. D **96**, 035001 (2017).
[17] S. Nussinov, Technocosmology–Could a technibaryon excess provide a "Natural" missing mass candidate?, Phys. Lett. **165B**, 55 (1985).
[18] D. B. Kaplan, A Single Explanation for Both the Baryon and Dark Matter Densities, Phys. Rev. Lett. **68**, 741 (1992).
[19] D. Hooper, J. March-Russell, and Stephen M. West, Asymmetric sneutrino dark matter and the $\Omega_b/\Omega_{\rm DM}$ puzzle, Phys. Lett. B **605**, 228 (2005).
[20] D. E. Kaplan, M. A. Luty, and K. M. Zurek, Asymmetric dark matter, Phys. Rev. D **79**, 115016 (2009).
[21] K. Petraki and R. R. Volkas, Review of asymmetric dark matter, Int. J. Mod. Phys. A **28**, 1330028 (2013).
[22] K. M. Zurek, Asymmetric dark matter: Theories, signatures, and constraints, Phys. Rep. **537**, 91 (2014).
[23] B. P. Abbott *et al.* (LIGO Scientific and Virgo Collaborations), Observation of Gravitational Waves from a Binary Black Hole Merger, Phys. Rev. Lett. **116**, 061102 (2016).
[24] P. Amaro-Seoane *et al.* (LISA Collaboration), Laser interferometer space antenna, arXiv:1702.00786.
[25] J. Crowder and N. J. Cornish, Beyond LISA: Exploring future gravitational wave missions, Phys. Rev. D **72**, 083005 (2005).
[26] S. Kawamura *et al.*, The Japanese space gravitational wave antenna: DECIGO, Classical Quantum Gravity **28**, 094011 (2011).
[27] M. Punturo *et al.*, The Einstein telescope: A third-generation gravitational wave observatory, Classical Quantum Gravity **27**, 194002 (2010).
[28] D. Reitze *et al.*, Cosmic Explorer: The U.S. contribution to gravitational-wave astronomy beyond LIGO, Bull. Am. Astron. Soc. **51**, 035 (2019), https://baas.aas.org/pub/2020n7i035/release/1.

[29] A. Kosowsky, M. S. Turner, and R. Watkins, Gravitational radiation from colliding vacuum bubbles, Phys. Rev. D **45**, 4514 (1992).
[30] M. S. Turner, Detectability of inflation produced gravitational waves, Phys. Rev. D **55**, R435 (1997).
[31] T. Hiramatsu, M. Kawasaki, and K. Saikawa, Gravitational waves from collapsing domain walls, J. Cosmol. Astropart. Phys. 05 (2010) 032.
[32] T. Vachaspati and A. Vilenkin, Gravitational radiation from cosmic strings, Phys. Rev. D **31**, 3052 (1985).
[33] M. Sakellariadou, Gravitational waves emitted from infinite strings, Phys. Rev. D **42**, 354 (1990); **43**, 4150(E) (1991).
[34] T. W. B. Kibble, Topology of cosmic domains and strings, J. Phys. A **9**, 1387 (1976).
[35] M. Eto, M. Kurachi, and M. Nitta, Constraints on two Higgs doublet models from domain walls, Phys. Lett. B **785**, 447 (2018).
[36] M. Eto, M. Kurachi, and M. Nitta, Non-Abelian strings and domain walls in two Higgs doublet models, J. High Energy Phys. 08 (2018) 195.
[37] N. Chen, T. Li, Z. Teng, and Y. Wu, Collapsing domain walls in the two-Higgs-doublet model and deep insights from the EDM, J. High Energy Phys. 10 (2020) 081.
[38] R. A. Battye, A. Pilaftsis, and D. G. Viatic, Domain wall constraints on two-Higgs-doublet models with Z_2 symmetry, Phys. Rev. D **102**, 123536 (2020).
[39] K. Kadota, M. Kawasaki, and K. Saikawa, Gravitational waves from domain walls in the next-to-minimal supersymmetric standard model, J. Cosmol. Astropart. Phys. 10 (2015) 041.
[40] N. Craig, I. Garcia Garcia, G. Koszegi, and A. McCune, P not PQ, J. High Energy Phys. 09 (2021) 130.
[41] G. B. Gelmini, A. Simpson, and E. Vitagliano, Gravitational waves from axionlike particle cosmic string-wall networks, Phys. Rev. D **104**, 061301 (2021).
[42] R. Z. Ferreira, A. Notari, O. Pujolas, and F. Rompineve, High Quality QCD Axion at Gravitational Wave Observatories, Phys. Rev. Lett. **128**, 141101 (2022).
[43] G. B. Gelmini, A. Simpson, and E. Vitagliano, Catastrogenesis: DM, GWs, and PBHs from ALP string-wall networks, J. Cosmol. Astropart. Phys. 02 (2023) 031.
[44] S. Blasi, A. Mariotti, A. Rase, A. Sevrin, and K. Turbang, Friction on ALP domain walls and gravitational waves, J. Cosmol. Astropart. Phys. 04 (**2023**) 008.
[45] B. Barman, D. Borah, A. Dasgupta, and A. Ghoshal, Probing high scale dirac leptogenesis via gravitational waves from domain walls, Phys. Rev. D **106**, 015007 (2022).
[46] D. Borah and A. Dasgupta, Probing left-right symmetry via gravitational waves from domain walls, Phys. Rev. D **106**, 035016 (2022).
[47] Z. A. Borboruah and U. A. Yajnik, Left-right symmetry breaking and gravitational waves: A tale of two phase transitions, arXiv:2212.05829.
[48] G. B. Gelmini, S. Pascoli, E. Vitagliano, and Y.-L. Zhou, Gravitational wave signatures from discrete flavor symmetries, J. Cosmol. Astropart. Phys. 02 (2021) 032.
[49] D. I. Dunsky, A. Ghoshal, H. Murayama, Y. Sakakihara, and G. White, Gravitational wave gastronomy, Phys. Rev. D 1 **106**, 075030 (2022).
[50] T. Moroi and K. Nakayama, Domain walls and gravitational waves after thermal inflation, Phys. Lett. B **703**, 160 (2011).
[51] K. Saikawa, A review of gravitational waves from cosmic domain walls, Universe **3**, 40 (2017).
[52] C. Grojean and G. Servant, Gravitational waves from phase transitions at the electroweak scale and beyond, Phys. Rev. D **75**, 043507 (2007).
[53] V. Vaskonen, Electroweak baryogenesis and gravitational waves from a real scalar singlet, Phys. Rev. D **95**, 123515 (2017).
[54] G. C. Dorsch, S. J. Huber, T. Konstandin, and J. M. No, A second Higgs doublet in the early universe: Baryogenesis and gravitational waves, J. Cosmol. Astropart. Phys. 05 (2017) 052.
[55] J. Bernon, L. Bian, and Y. Jiang, A new insight into the phase transition in the early universe with two Higgs doublets, J. High Energy Phys. 05 (2018) 151.
[56] I. Baldes and G. Servant, High scale electroweak phase transition: Baryogenesis and symmetry non-restoration, J. High Energy Phys. 10 (2018) 053.
[57] M. Chala, C. Krause, and G. Nardini, Signals of the electroweak phase transition at colliders and gravitational wave observatories, J. High Energy Phys. 07 (2018) 062.
[58] A. Alves, T. Ghosh, H.-K. Guo, K. Sinha, and D. Vagie, Collider and gravitational wave complementarity in exploring the singlet extension of the standard model, J. High Energy Phys. 04 (2019) 052.
[59] X.-F. Han, L. Wang, and Y. Zhang, Dark matter, electroweak phase transition, and gravitational waves in the Type II two-Higgs-doublet model with a singlet scalar field, Phys. Rev. D **103**, 035012 (2021).
[60] N. Benincasa, L. Delle Rose, K. Kannike, and L. Marzola, Multistep phase transitions and gravitational waves in the inert doublet model, J. Cosmol. Astropart. Phys. 12 (2022) 025.
[61] P. Schwaller, Gravitational Waves from a Dark Phase Transition, Phys. Rev. Lett. **115**, 181101 (2015).
[62] M. Breitbach, J. Kopp, E. Madge, T. Opferkuch, and P. Schwaller, Dark, cold, and noisy: Constraining secluded hidden sectors with gravitational waves, J. Cosmol. Astropart. Phys. 07 (2019) 007.
[63] D. Croon, V. Sanz, and G. White, Model discrimination in gravitational wave spectra from dark phase transitions, J. High Energy Phys. 08 (**2018**) 203.
[64] E. Hall, T. Konstandin, R. McGehee, H. Murayama, and G. Servant, Baryogenesis from a dark first-order phase transition, J. High Energy Phys. 04 (2020) 042.
[65] I. Baldes, Gravitational waves from the asymmetric-dark-matter generating phase transition, J. Cosmol. Astropart. Phys. 05 (2017) 028.
[66] A. Azatov, M. Vanvlasselaer, and W. Yin, Dark matter production from relativistic bubble walls, J. High Energy Phys. 03 (2021) 288.
[67] F. Costa, S. Khan, and J. Kim, A two-component dark matter model and its associated gravitational waves, J. High Energy Phys. 06 (**2022**) 026.
[68] F. Costa, S. Khan, and J. Kim, A two-component vector WIMP—fermion FIMP dark matter model with an extended seesaw mechanism, J. High Energy Phys. 12 (2022) 165.

[69] B. Fornal and E. Pierre, Asymmetric dark matter from gravitational waves, Phys. Rev. D **106**, 115040 (2022).
[70] M. Kierkla, A. Karam, and B. Swiezewska, Conformal model for gravitational waves and dark matter: A status update, J. High Energy Phys. 03 (2023) 007.
[71] A. Azatov, G. Barni, S. Chakraborty, M. Vanvlasselaer, and W. Yin, Ultra-relativistic Bubbles from the simplest Higgs portal and their cosmological consequences, J. High Energy Phys. 10 (2022) 017.
[72] P. S. B. Dev, F. Ferrer, Y. Zhang, and Y. Zhang, Gravitational waves from first-order phase transition in a simple axion-like particle model, J. Cosmol. Astropart. Phys. 11 (2019) 006.
[73] B. Von Harling, A. Pomarol, O. Pujolas, and F. Rompineve, Peccei-Quinn phase transition at LIGO, J. High Energy Phys. 04 (**2020**) 195.
[74] L. Delle Rose, G. Panico, M. Redi, and A. Tesi, Gravitational waves from supercool axions, J. High Energy Phys. 04 (2020) 025.
[75] D. Croon, T. E. Gonzalo, and G. White, Gravitational waves from a Pati-Salam phase transition, J. High Energy Phys. 02 (2019) 083.
[76] W.-C. Huang, F. Sannino, and Z.-W. Wang, Gravitational waves from Pati-Salam dynamics, Phys. Rev. D **102**, 095025 (2020).
[77] N. Okada, O. Seto, and H. Uchida, Gravitational waves from breaking of an extra $U(1)$ in $SO(10)$ grand unification, Prog. Theor. Exp. Phys. **2021**, 033B01 (2021).
[78] J. Ellis, M. Lewicki, and V. Vaskonen, Updated predictions for gravitational waves produced in a strongly supercooled phase transition, J. Cosmol. Astropart. Phys. 11 (2020) 020.
[79] K. Kawana, Cosmology of a supercooled universe, Phys. Rev. D **105**, 103515 (2022).
[80] N. Craig, N. Levi, A. Mariotti, and D. Redigolo, Ripples in spacetime from broken supersymmetry, J. High Energy Phys. 02 (2020) 184.
[81] B. Fornal, B. Shams Es Haghi, J.-H. Yu, and Y. Zhao, Gravitational waves from mini-split SUSY, Phys. Rev. D **104**, 115005 (2021).
[82] V. Brdar, L. Graf, A. J. Helmboldt, and X.-J. Xu, Gravitational waves as a probe of left-right symmetry breaking, J. Cosmol. Astropart. Phys. 12 (2019) 027.
[83] L. Graf, S. Jana, A. Kaladharan, and S. Saad, Gravitational wave imprints of left-right symmetric model with minimal Higgs sector, J. Cosmol. Astropart. Phys. 05 (2022) 003.
[84] V. Brdar, A. J. Helmboldt, and J. Kubo, Gravitational waves from first-order phase transitions: LIGO as a window to unexplored seesaw scales, J. Cosmol. Astropart. Phys. 02 (2019) 021.
[85] N. Okada and O. Seto, Probing the seesaw scale with gravitational waves, Phys. Rev. D **98**, 063532 (2018).
[86] P. Di Bari, D. Marfatia, and Y.-L. Zhou, Gravitational waves from first-order phase transitions in majoron models of neutrino mass, J. High Energy Phys. 10 (2021) 193.
[87] R. Zhou, L. Bian, and Y. Du, Electroweak phase transition and gravitational waves in the Type-II seesaw model, J. High Energy Phys. 08 (**2022**) 205.
[88] T. Hasegawa, N. Okada, and O. Seto, Gravitational waves from the minimal gauged $U(1)_{B-L}$ model, Phys. Rev. D **99**, 095039 (2019).
[89] B. Fornal and B. Shams Es Haghi, Baryon and lepton number violation from gravitational waves, Phys. Rev. D **102**, 115037 (2020).
[90] A. Greljo, T. Opferkuch, and B. A. Stefanek, Gravitational Imprints of Flavor Hierarchies, Phys. Rev. Lett. **124**, 171802 (2020).
[91] B. Fornal, Gravitational wave signatures of lepton universality violation, Phys. Rev. D **103**, 015018 (2021).
[92] A. Dasgupta, P. S. B. Dev, A. Ghoshal, and A. Mazumdar, Gravitational wave pathway to testable leptogenesis, Phys. Rev. D **106**, 075027 (2022).
[93] E. J. Chun, T. P. Dutka, T. H. Jung, X. Nagels, and M. Vanvlasselaer, Bubble-assisted leptogenesis, arXiv:2305.10759.
[94] J. Ellis, M. Lewicki, J. M. No, and V. Vaskonen, Gravitational wave energy budget in strongly supercooled phase transitions, J. Cosmol. Astropart. Phys. 06 (2019) 024.
[95] M. Lewicki and V. Vaskonen, On bubble collisions in strongly supercooled phase transitions, Phys. Dark Universe **30**, 100672 (2020).
[96] M. Lewicki and V. Vaskonen, Gravitational wave spectra from strongly supercooled phase transitions, Eur. Phys. J. C **80**, 1003 (2020).
[97] C. Badger, B. Fornal, K. Martinovic, A. Romero, K. Turbang, H. Guo, A. Mariotti, M. Sakellariadou, A. Sevrin, F.-W. Yang, and Y. Zhao, Probing early universe supercooled phase transitions with gravitational wave data, Phys. Rev. D **107**, 023511 (2023).
[98] R. Caldwell *et al.*, Detection of early-universe gravitational-wave signatures and fundamental physics, Gen. Relativ. Gravit. **54**, 156 (2022).
[99] P. Athron, C. Balazs, A. Fowlie, L. Morris, and L. Wu, Cosmological phase transitions: From perturbative particle physics to gravitational waves, arXiv:2305.02357.
[100] B. Fornal and B. Grinstein, Dark Matter Interpretation of the Neutron Decay Anomaly, Phys. Rev. Lett. **120**, 191801 (2018); **124**, 219901(E) (2020).
[101] Wolfram Research, Inc., Wolfram Programming Lab, Version 13.2, Champaign, IL, 2023.
[102] K. Dick, M. Lindner, M. Ratz, and D. Wright, Leptogenesis with Dirac Neutrinos, Phys. Rev. Lett. **84**, 4039 (2000).
[103] H. Murayama and A. Pierce, Realistic Dirac Leptogenesis, Phys. Rev. Lett. **89**, 271601 (2002).
[104] J. Shu, T. M. P. Tait, and C. E. M. Wagner, Baryogenesis from an earlier phase transition, Phys. Rev. D **75**, 063510 (2007).
[105] M. Blennow, B. Dasgupta, E. Fernandez-Martinez, and N. Rius, Aidnogenesis via leptogenesis and dark sphalerons, J. High Energy Phys. 03 (2011) 014.
[106] I. F. Ginzburg and M. Krawczyk, Symmetries of two Higgs doublet model and *CP* violation, Phys. Rev. D **72**, 115013 (2005).
[107] R. A. Battye, G. D. Brawn, and A. Pilaftsis, Vacuum topology of the two Higgs doublet model, J. High Energy Phys. 08 (2011) 020.
[108] M. Joyce, T. Prokopec, and N. Turok, Nonlocal electroweak baryogenesis. Part 1: Thin wall regime, Phys. Rev. D **53**, 2930 (1996).

[109] A. G. Cohen, D. B. Kaplan, and A. E. Nelson, Diffusion enhances spontaneous electroweak baryogenesis, Phys. Lett. B **336**, 41 (1994).
[110] A. Riotto, Towards a nonequilibrium quantum field theory approach to electroweak baryogenesis, Phys. Rev. D **53**, 5834 (1996).
[111] J. A. Harvey and M. S. Turner, Cosmological baryon and lepton number in the presence of electroweak fermion number violation, Phys. Rev. D **42**, 3344 (1990).
[112] R. L. Workman *et al.* (Particle Data Group), Review of particle physics, Prog. Theor. Exp. Phys. **2022**, 083C01 (2022).
[113] T. Hiramatsu, M. Kawasaki, and K. Saikawa, On the estimation of gravitational wave spectrum from cosmic domain walls, J. Cosmol. Astropart. Phys. 02 (2014) 031.
[114] T. J. Clarke, E. J. Copeland, and A. Moss, Constraints on primordial gravitational waves from the cosmic microwave background, J. Cosmol. Astropart. Phys. 10 (2020) 002.
[115] G. W. Anderson and L. J. Hall, The electroweak phase transition and baryogenesis, Phys. Rev. D **45**, 2685 (1992).
[116] M. Quiros, Field theory at finite temperature and phase transitions, Acta Phys. Pol. B **38**, 3661 (2007), https://www.actaphys.uj.edu.pl/fulltext?series=Reg&vol=38&page=3661.
[117] D. Comelli and J. R. Espinosa, Bosonic thermal masses in supersymmetry, Phys. Rev. D **55**, 6253 (1997).
[118] A. D. Linde, Decay of the false vacuum at finite temperature, Nucl. Phys. **B216**, 421 (1983).
[119] J. R. Espinosa, T. Konstandin, J. M. No, and G. Servant, Energy budget of cosmological first-order phase transitions, J. Cosmol. Astropart. Phys. 06 (2010) 028.
[120] C. Caprini *et al.*, Science with the space-based interferometer eLISA. II: Gravitational waves from cosmological phase transitions, J. Cosmol. Astropart. Phys. 04 (2016) 001.
[121] M. Hindmarsh, S. J. Huber, K. Rummukainen, and D. J. Weir, Gravitational Waves from the Sound of a First Order Phase Transition, Phys. Rev. Lett. **112**, 041301 (2014).
[122] J. Ellis, M. Lewicki, and J. M. No, Gravitational waves from first-order cosmological phase transitions: Lifetime of the sound wave source, J. Cosmol. Astropart. Phys. 07 (2020) 050.
[123] H.-K. Guo, K. Sinha, D. Vagie, and G. White, Phase transitions in an expanding universe: Stochastic gravitational waves in standard and non-standard histories, J. Cosmol. Astropart. Phys. 01 (**2021**) 001.
[124] S. J. Huber and T. Konstandin, Gravitational wave production by collisions: More bubbles, J. Cosmol. Astropart. Phys. 09 (2008) 022.
[125] M. Lewicki and V. Vaskonen, Gravitational waves from colliding vacuum bubbles in gauge theories, Eur. Phys. J. C **81**, 437 (2021).
[126] M. Kamionkowski, A. Kosowsky, and M. S. Turner, Gravitational radiation from first order phase transitions, Phys. Rev. D **49**, 2837 (1994).
[127] C. Caprini and R. Durrer, Gravitational waves from stochastic relativistic sources: Primordial turbulence and magnetic fields, Phys. Rev. D **74**, 063521 (2006).
[128] C. Caprini, R. Durrer, and G. Servant, The stochastic gravitational wave background from turbulence and magnetic fields generated by a first-order phase transition, J. Cosmol. Astropart. Phys. 12 (**2009**) 024.
[129] A. Vilenkin and E. P. S. Shellard, *Cosmic Strings and Other Topological Defects* (Cambridge University Press, Cambridge, England, 2000).
[130] Y. Gouttenoire, G. Servant, and P. Simakachorn, Beyond the standard models with cosmic strings, J. Cosmol. Astropart. Phys. 07 (2020) 032.
[131] Qaisar Shafi (private communication).
[132] M. Hindmarsh, K. Rummukainen, and D. J. Weir, New Solutions for Non-Abelian Cosmic Strings, Phys. Rev. Lett. **117**, 251601 (2016).
[133] J. Bosch, Z. Delgado, B. Fornal, and A. Leon, Gravitational wave signatures of gauged baryon and lepton number, arXiv:2306.00332.